Optimisation of pH of the CdCl2+Ga2(SO4)3 activation step of CdS/CdTe based thin-film solar cells

OJO, A.A. and DHARMADASA, I <http://orcid.org/0000-0001-7988-669X>

Optimisation of pH of the $CdCl_2$+$Ga_2(SO_4)_3$ Activation Step of CdS/CdTe Based Thin-Film Solar Cells

A.A. Ojo* and I.M. Dharmadasa
Electronic Materials and Sensors Group, Materials and Engineering Research Institute (MERI), Sheffield Hallam University, Sheffield S1 1WB, UK.
*Email: chartell2006@yahoo.com; Tel: +44 114 225 6910 Fax: +44 114 225 6930

Abstract

In order to produce high efficiency solar cells based on CdTe, $CdCl_2$ post-growth treatment is an essential processing step. This treatment can be further improved by adding elements such as Fluorine and Gallium into the $CdCl_2$ solution. Through systematic experimentation, it has been found that the pH value of the treatment solution also affect the conversion efficiency of the solar cells. This work therefore focuses on the effect of pH value of $CdCl_2$+$Ga_2(SO_4)_3$ aqueous solution on the device efficiencies. The graded bandgap device structure, glass/FTO/*n*-ZnS/*n*-CdS/*n*-CdTe/Au was used in this work. The pH values of 1.00, 2.00 and 3.00 for $CdCl_2$+$Ga_2(SO_4)_3$ solutions were utilised for the activation of glass/FTO/*n*-ZnS/*n*-CdS/*n*-CdTe layers and its effects were explored for both the CdTe material and device properties. It has been found that both CdTe material properties and solar cell device properties are superior when the pH value of 2.00 is used for post-growth treatment. The best conversion efficiency observed in this work for the above graded bandgap device is 12.2%.

Keywords: Graded bandgap, $CdCl_2$+$Ga_2(SO_4)_3$, ZnS/CdS/CdTe, postgrowth treatment, pH.

1 Introduction

Tellurium (Te) precipitation in cadmium telluride (CdTe) has been a known issue in CdTe layers irrespective of the growth technique (Fernández, 2003). An integral part of achieving a reduction in Te precipitation and highly efficient solar cells has been dependent on the post-growth treatment (PGT) of CdTe in the presence of excess Cd, chlorine (Dharmadasa, 2014) and fluorine (Rios-Flores et al., 2012) ($CdCl_2$ treatment). Amongst the advantages associated with PGT includes the improvement in grain growth, recrystallisation, optical property, electrical conductivity, doping concentration, grain boundary passivation, improved Cd/Te composition, CdS/CdTe interface morphology (Basol, 1992; Bosio et al., 2006; Dharmadasa et al., 2017; Liu et al., 2015; Xue et al., 2016) and reduction in native defects (I. M. Dharmadasa et al., 2015). Different post-growth treatments have been utilised for the improvement of the characteristic properties of CdTe as documented in the literature (Major et al., 2016, 2015; Mis-Fernández et al., 2017; Williams et al., 2015). Based on the ability of gallium to dissolve Te-precipitates in CdTe (Fernández, 2003; Sochinskii et al., 1993), our previous research work has been focused on its incorporation in the usual $CdCl_2$ treatment of CdTe (Ojo et al., 2017; Olusola et al., 2017) from which high-efficiency CdS/CdTe-based devices were fabricated with improved material and electronic properties. So far, the effect of pH on the $CdCl_2$+$Ga_2(SO_4)_3$ (GCT) post-growth treatment of CdS/CdTe based solar cell is yet unknown. In the present study, the focus was on the effect of pH on the $CdCl_2$+$Ga_2(SO_4)_3$ PGT with the aim to further improve both the material and electronic properties of glass/FTO/*n*-ZnS/*n*-CdS/*n*-CdTe/Au devices fabricated.

2 Experimental details

All the chemicals and glass/FTO substrates utilised in this sets of experiments were bought from Sigma Aldrich UK. Two-electrode electroplating technique was employed for all the deposited semiconductors utilised in this work in which a high purity graphite electrode is the anode, and transparent conducting oxide (TCO) was used as the cathode. The specification of the glass/fluorine-doped tin oxide (FTO) utilised in this work is TEC-7 with a sheet resistance of ~7 Ω/□. Prior to the electroplating, the glass/FTO substrates were cut into 4×3 cm^2, ultrasonically washed for 15 min in soap water, rinsed in deionised (DI) water, degreased using acetone and rinsed afterwards in a flow of DI water. Before the transfer of the glass/FTO into the electrolytic bath, the substrate is attached to a high purity graphite rod using polytetrafluoroethylene (PTFE) tape but only the FTO surface was in contact with the electrolyte. A computerised GillAC potentiostat was utilised as the power supply source.

2.1 Sample preparation

The *n*-ZnS buffer layer was electrodeposited (ED) on the glass/FTO substrates from an electrolyte containing zinc sulphate monohydrate ($ZnSO_4 \cdot H_2O$) and ammonium thiosulphate ($(NH_4)_2S_2O_3$) with respective purity of 99.9% and 98%. The electrolytic bath was prepared by mixing 0.2 M $ZnSO_4 \cdot H_2O$ and 0.2 M $(NH_4)_2S_2O_3$ aqueous solutions in 400 ml plastic vessel to use as zinc and sulphur precursors respectively. For this work, 50 nm thick *n*-ZnS layers were electroplated at a cathodic voltage of 1425 mV close to the *p*-to-*n* conduction type transition voltage (V_i). Details of the ED-ZnS has been documented in the literature (Madugu et al., 2016). The electrodeposited glass/FTO/*n*-ZnS layers were annealed in air at 300°C and air-cooled afterwards. It should be noted that the conduction type of the *n*-ZnS is retained after annealing (Madugu et al., 2016).

65 nm thick *n*-CdS window layers were electroplated on the post-growth treated glass/FTO/*n*-ZnS layers. The CdS was electroplated from an aqueous electrolyte containing 0.3 M hydrated cadmium chloride ($CdCl_2 \cdot xH_2O$) and 0.03 M ammonium thiosulphate ($(NH_4)_2S_2O_3$) with respective purity of 99.99% and 98% in 400 ml of DI water. The CdS layers were deposited at a pre-optimised cathodic voltage of 1200 mV (Abdul-Manaf et al., 2015). The deposited glass/FTO/*n*-ZnS/*n*-CdS structure was annealed in the presence of $CdCl_2$. The $CdCl_2$ treatment was performed by adding few drops of aqueous solution containing 0.1 M $CdCl_2$ in 20 ml of DI water to the surface of the semiconductor layer. The full coverage of the layers with the treatment solutions was achieved by spreading the solution using solution-damped cotton bud. The semiconductor layer was allowed to air-dry and heat treated at 400°C for 20 min. The treated glass/FTO/*n*-ZnS/*n*-CdS layers were air-cooled and rinsed in DI water before *n*-CdTe layer deposition. Full details of deposition and optimisation of ED-CdS layer has been published in the literature (Abdul-Manaf et al., 2015). It should be noted that CdS layers are intrinsically *n*-type due defects related to Cd interstitials and S vacancies in CdS layers (Sathaye and Sinha, 1976).

1150 nm thick *n*-CdTe layers were electrodeposited at 1400 mV on the glass/FTO/*n*-ZnS/*n*-CdS substrate. The CdTe layers were deposited from an electrolyte containing 1.5 M cadmium nitrate tetrahydrate ($Cd(NO_3)_2 \cdot 4H_2O$) and 0.0023 M tellurium dioxide (TeO_2) with respective purity of 99.0% and 99.99% in 400 ml of deionised water. Full details of deposition, characterisation and optimisation of the electroplated CdTe layers has been documented in the literature (Salim et al., 2015). Prior to GCT activation process of the glass/FTO/*n*-ZnS/*n*-CdS/*n*-CdTe, the 4×3 cm^2 glass/FTO/*n*-ZnS/*n*-CdS/*n*-CdTe layers were cut into 3 sets of 4×1 cm^2 samples.

The $CdCl_2$+$Ga_2(SO_4)_3$ solution utilised for the GCT was prepared in aqueous solution containing 0.1 M $CdCl_2$ and 0.05 M $Ga_2(SO_4)_3$ in a 60 ml of DI water. The solution was stirred for 60 min to achieve homogeneity and 20 ml of the solution was poured into three different 25 ml glass beakers. The pH of the $CdCl_2$+$Ga_2(SO_4)_3$ solutions were adjusted to 1.00±0.02, 2.00±0.02 and 3.00±0.02 using dilute HCl solution. Afterwards, the glass/FTO/*n*-ZnS/*n*-CdS/*n*-CdTe layers were treated using $CdCl_2$+$Ga_2(SO_4)_3$ solutions of different pH, dried in air and heat treated at 400℃ for 20 min in air atmosphere (Ojo et al., 2017). The full coverage of the layers was achieved by the use of solution damped cotton buds.

The annealed glass/FTO/*n*-ZnS/*n*-CdS/*n*-CdTe layers were etched using aqueous solutions containing H_2SO_4 and $K_2Cr_2O_7$ for acid etching, and NaOH and $Na_2S_2O_3$ for alkaline etching for 2 s and 2 min respectively to improve the metal/semiconductor contact (Dharmadasa et al., 1998). The glass/FTO/*n*-ZnS/*n*-CdS/*n*-CdTe layers were immediately transferred to a high vacuum system to deposit 100 nm thick Au contacts of 2 mm diameter on the glass/FTO/*n*-ZnS/*n*-CdS/*n*-CdTe structure at a low pressure of 10^{-5} Nm^{-2}.

2.2 Graded bandgap configuration

The basic concept behind graded bandgap (GBG) solar cell is the possibility of effective harnessing of photons across the ultraviolet (UV), visible (Vis) and infrared (IR) regions (Dharmadasa, 2005). This concept has been validated in the literature across organic (Ergen et al., 2016), inorganic (Dharmadasa et al., 2011; I.M. Dharmadasa et al., 2015) and hybrid (Dharmadasa, 2005; Ergen et al., 2016) solar cell technology. Graded bandgap can be achieved by grading the semiconductor layers in such a way that the bandgap varies throughout the entire thickness (Dharmadasa et al., 2011). GBG can also be produced by successively growing semiconductor materials on top of each other in which the layers are arranged such that the bandgap decreases gradually while the conductivity type gradually changes from one type to the other (Dharmadasa, 2005).

The earliest work that theoretically described the functionality of GBG configuration was reported by Tauc in 1957 (Tauc, 1957). His work elucidates the possibility of GBG solar cell configuration attaining higher conversion efficiency above the well-explored *p*-*n* junction cells stimulated interest in the photovoltaic research community. Taking into consideration the photogenerated current, it was proven theoretically that GBG solar cell configurations are capable of attaining a conversion efficiency of ~38% under AM1.5 (Emtage, 1962; Wolf, 1960) as compared to the 23% of single *p*-*n* junction solar cells. Based on this theoretical understanding, the first sets of graded bandgap cells were fabricated and reported in the

1970s (Hovel and Woodall, 1973; Konagai and Takahashi, 1975) by gradual doping of only *p*-type gallium arsenide (GaAs) with aluminium. The published work demonstrated a single-sided *p*-type grading of *p*-$Ga_{1-x}Al_xAs$/*n*-GaAs solar cell. In 2002, the first model of full solar cell device bandgap grading was proposed and published by Dharmadasa et al (Dharmadasa et al., 2002). The full graded bandgap (GBG) architectures as proposed in the literature (Dharmadasa et al., 2005; Dharmadasa, 2005) can be accomplished by the incorporation of either an *n*-type or *p*-type wide bandgap front-layer with a steady reduction in bandgap towards *p*-type or *n*-type back layer respectively.

The glass/FTO/*n*-ZnS/*n*-CdS/*n*-CdTe/Au graded bandgap configuration examined in this work (see Figure 1) is relative to the technology as documented in the literature (Dharmadasa et al., 2005). It should be noted that the incorporated semiconductor layers (ZnS, CdS, and CdTe) have been individually examined and documented in the literature (Abdul-Manaf et al., 2015; Madugu et al., 2016; Salim et al., 2015). Asides from the bandgap grading of ZnS (3.72 eV (Madugu et al., 2016)), CdS (2.42 eV (Abdul-Manaf et al., 2015)), and CdTe (1.50 eV (Salim et al., 2015)), there are possible formation of $Zn_xCd_{1-x}S$ and CdS_xTe_{1-x} ternary compounds in-between successively deposited semiconductor layers due to interface interaction and chemical reactions. Literature on bandgap grading based on incorporated ZnS/CdS/CdTe layers have been well established in the literature (Han et al., 2013; Oladeji and Chow, 2005).

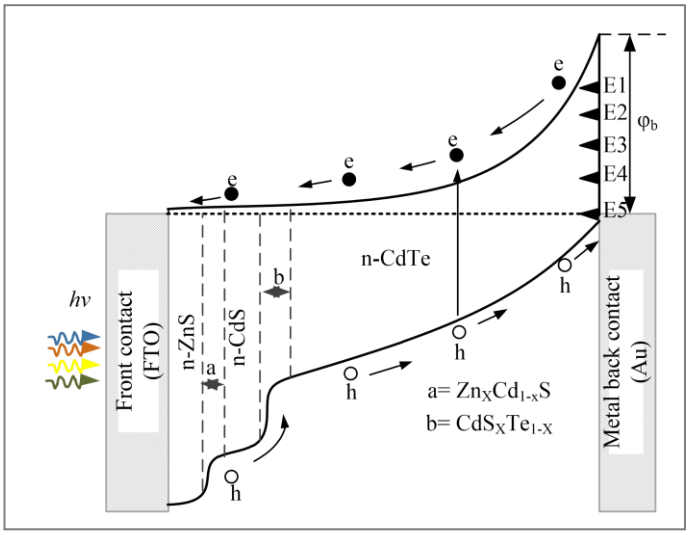

Figure 1: A typical band diagram of graded bandgap glass/FTO/*n*-ZnS/*n*-CdS/*n*-CdTe/Au device configuration.

As documented in the literature, the formation of such ternary compound is attributable to the interdiffusion of elemental Zn & Cd across the ZnS/CdS interface (Oladeji and Chow, 2005) and S & Te (Li et al., 2014) across the CdS/CdTe interface during the post-growth treatment processes. The formed ternary compounds also participate in the bandgap grading due to continuous band bending as observed in Figure 1. Further to this, the *n*-CdTe/metal interface (Dharmadasa et al., 1998) creates a large Schottky barrier (SB), which provides the main electric field in the glass/FTO/*n*-ZnS/*n*-CdS/*n*-CdTe/Au GBG configuration. As shown in Figure 1, the effective separation of the photogenerated e-h pairs is achievable as depicted by the propagation of the depletion region across all the layers.

2.3 Characterisation techniques

The work reported in this manuscript is focused on device properties, but the mentioned material properties such as the analyses of both the morphology and composition of the deposited layers were studied using FEI Nova 200 NanoSEM equipment with an Energy-dispersive X-ray spectroscopy (EDX) compartment. The optical properties of the grown thin films were investigated at room temperature using Cary 50 Scan Ultraviolet-Visible (UV-Vis) spectrophotometer within the wavelength range of (200 – 1000) nm. X-ray diffraction (XRD) was utilised for acquiring information about the level of crystallinity, identification of elements, compounds and phases of the deposited layers. The XRD equipment utilised was Philips PW 3710 X'pert diffractometer with Cu-K_α monochromator of wavelength λ=1.54 Å. The X-ray generator tension and generator current were respectively set to 40 kV and 40 mA. The conduction types were determined using Photoelectrochemical (PEC) cell measurement. The layers utilised for the PEC measurement was 2×3 cm^2 glass/FTO/n-CdTe layer with a CdTe thickness of 1150 nm grown at 1400 mV. The DC conductivity measurements were carried out on glass/FTO/CdTe/ohmic contact structures using Rera Solution fully automated I-V system. Depending on the conduction type of the CdTe in the glass/FTO/CdTe layer after post-growth treatment, 100 nm thick Au was deposited on *p*-CdTe or Al on *n*-CdTe to achieve Ohmic contacts prior to DC conductivity measurements.

The main device characterisation techniques utilised for the analysis of the fabricated glass/FTO/*n*-ZnS/*n*-CdS/*n*-CdTe/Au devices were the current-voltage (I-V) and capacitance-voltage (C-V) methods. The I-V characterisations were performed under both dark and AM1.5 illuminated conditions using fully automated Rera Solution PV simulation system. The Rera Solution PV measurement system is comprised of a Keithley 2401 SourceMeter, LOT Quantum Design GmbH arc light source and a computer laptop running Rera Tracer IV

software. The system was calibrated before use, using RR267MON standard reference Si-based cell prior to measurements. The C-V measurements were carried out using fully automated HP 4284A Precision LCR meter at a detecting signal frequency of 1 MHz under dark condition. For both the I-V and C-V measurements, the bias range was set between −1.0 V and +1.0 V at 300 K for all the measurements taken.

3 The effects of pH value of the $CdCl_2$+$Ga_2(SO_4)_3$ treatment solution on properties of CdTe layer

Figure 2(a-c) show the respective morphology of the glass/FTO/*n*-ZnS/*n*-CdS/*n*-CdTe layers activated with GCT solution at pH1, pH2 and pH3. Figure 2(d) and Figure 2(e) show the compositional analysis and the photoelectrochemical (PEC) cell measurement results of the glass/FTO/CdTe activated with GCT solution at pH1, pH2, and pH3. Figure 2(f) and Figure 2(g) show the Tauc's plot, and the XRD diffraction of the glass/FTO/CdTe layers activated with GCT solution at pH1, pH2 and pH3. Further to the material summary captured in Figure 2, Figure 3 shows the point compositional EDX analysis on the glass/FTO/CdTe layer treated with pH1 GCT.

With respect to Figure 2(a-c), the morphology of the layers show the presence of large grains with sizes >2 µm as observed for samples treated with GCT of pH2, while samples treated with GCT of pH3 and pH1 show smaller grains size averaging ~1 µm. Consequently, the best underlying glass/FTO substrate coverage was observed for the glass/FTO/*n*-ZnS/*n*-CdS/*n*-CdTe layers treated with GCT pH3 followed by the pH2 and the pH1 treated layers. But the pH1 GCT treated layers show a striking erosion of surface, due to the harshness of the acidic concentration of the treatment solution. The presence of Te-rich strands was also observable due to the dissolution of elemental Cd from the CdTe layers as depicted in Figure 2(a) and Figure 3. It is well known that an introduction of an acidic media to CdTe attacks Cd preferentially leaving Te rich surface (Dharmadasa, 1998). In the case of the pH1 GCT treated layer, the layers were eroded leaving behind Te-rich surface and high pinhole density. The presence of high pinhole density of the pH1 GCT glass/FTO/*n*-ZnS/*n*-CdS/*n*-CdTe signifies the detrimental effect of the high acidity (low pH) of the treatment solution. It should also be taking into consideration that the grain growth observed after post-growth treatment of CdTe under favourable conditions are mainly attributed to the recrystallization, coalescence and Ostwald ripening of grains amongst other factors (Dharmadasa, 2014; McCandless and Sites, 2011). But due to the thinness of the films (within nano-scale), the nucleation mechanism of electrodeposited materials and the columnar growth nature of the

electroplated materials, the erosion of the CdTe surface will result in opening pores along the grain boundaries which may lead into shunt paths for charge carriers as in the case of pH1 GCT treated layer (see Figure 2(a)).

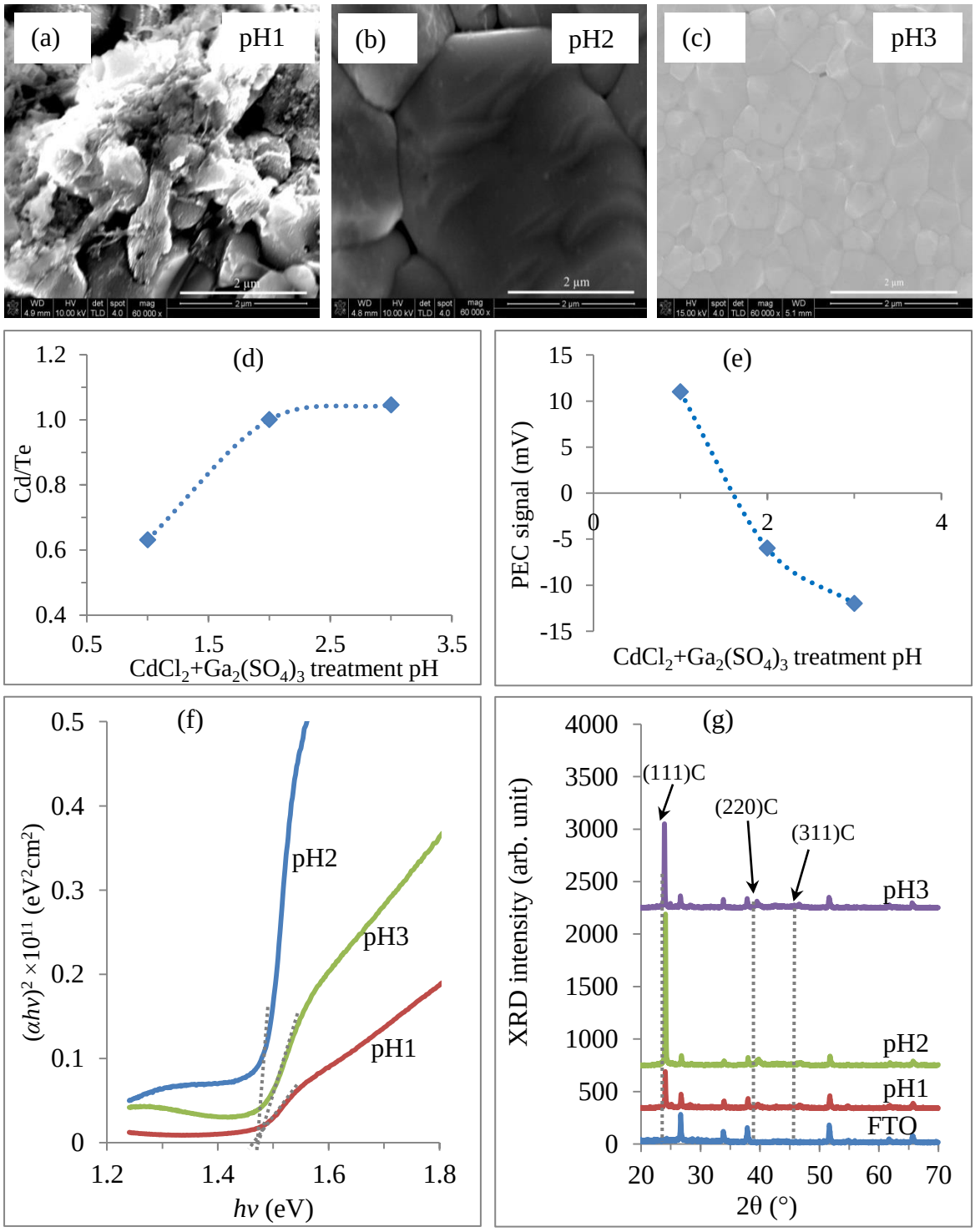

Figure 2: Typical results of SEM, EDX, PEC, optical absorption and XRD measurements for CdTe post-growth treated with pH1, pH2 and pH3 $CdCl_2$+$Ga_2(SO_4)_3$ solutions.

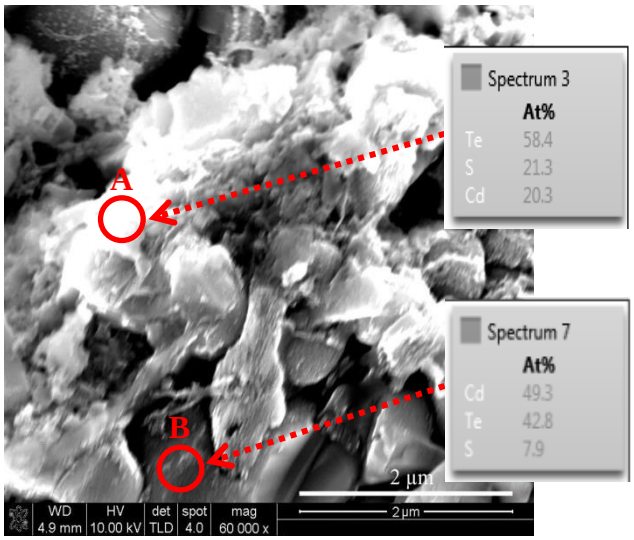

Figure 3: SEM micrograph of glass/FTO/*n*-ZnS/*n*-CdS/*n*-CdTe layers treated with GCT at pH1 and the EDX point micrographs on different parts of the CdTe layer; at points A (Te-rich) and B (nearly stoichiometric).

As regards the compositional analysis as shown in Figure 2(d), the observable trend of the Cd/Te ratio for the glass/FTO/*n*-ZnS/*n*-CdS/*n*-CdTe layers treated with GCT of pH3, pH2 and pH1 shows a >1.0, ~1.0 and <1.0 respectively. This observation can be attributed to the effect of increased acidity and acid etching resulting in the preferential dissolution of Cd from the CdTe surface (Dharmadasa, 2014; Williams et al., 2014). The alteration of the Cd to Te ratio from >1.0, tending towards ~1.0 and <1.0 for the glass/FTO/*n*-ZnS/*n*-CdS/*n*-CdTe layers treated with GCT of pH3, pH2 and pH1 are documented in the literature as one of the factors determining the conduction type of CdTe layers (Dharmadasa, 2014; Williams et al., 2014).

The photoelectrochemical cell measurement as shown in Figure 2(e) depicts a gradual transition of conduction type from p-type CdTe treated with pH1 GCT, to *n*-type CdTe treated with pH2 GCT (but close to *p*-type) and to an n-type conduction type for the glass/FTO/CdTe layers treated with pH3 GCT. It was therefore interesting to observe that the PEC cell measurements as shown in Figure 2(e) is in accord with the summations of the compositional analysis. The Te-rich CdTe surfaces show p-type electrical conduction and Cd-rich CdTe surfaces show n-type electrical conduction. It should be noted that the determination of conduction type and the possible transition of one conduction type to another after heat treatment of CdTe is not just determined by the composition of Cd/Te. Other factors documented in the literature include the doping effect caused by pre-annealing treatment, annealing duration and temperature, the initial atomic composition of Cd/Te, the

structure of the defect in the initial CdTe layer and the initial conductivity type of the material (Basol, 1992; Dharmadasa, 2014; Salim et al., 2015).

Pertaining to Figure 2(f), the absorbance for the glass/FTO/*n*-ZnS/*n*-CdS/*n*-CdTe layers activated with GCT of pH1, pH2 and pH3 was observed from Tauc's plot of $(\alpha hv)^2$ against hv where α is the absorption coefficient, h is the plank's constant and v is the incident photon frequency and λ is the wavelength (Tauc, 1968). Based on observation, all the glass/FTO/*n*-ZnS/*n*-CdS/*n*-CdTe layers with treated GCT pH1, pH2 and pH3 all show a bandgap of ~1.47±0.01 eV. The observed bandgaps are comparative to the bandgap of bulk CdTe. More importantly, the sharpness of the absorption edge slope for all the glass/FTO/*n*-ZnS/*n*-CdS/*n*-CdTe layers differs (see Figure 2(f)). As documented in the literature, the steeper the absorption edge the more the superiority of the semiconductor layer is based on lesser impurity energy levels and defects in the thin film (Bosio et al., 2006). Based on this submission, it could be interpreted that the glass/FTO/*n*-ZnS/*n*-CdS/*n*-CdTe layers activated with pH2 GCT are superior to others.

The structural analysis performed using XRD is depicted in Figure 2(g) with the plot of XRD diffraction intensity against 2θ°. The XRD patterns shown in Figure 2(g) were stacked for better comparison. The presence of (111), (220) and (311) cubic CdTe at 2θ=~23.8°, 2θ=~38.6° and 2θ=~45.8° were observed in all the XRD diffractions for all the glass/FTO/*n*-ZnS/*n*-CdS/*n*-CdTe layers activated with pH1, pH2 and pH3 GCT. It should be noted that the XRD diffraction patterns, other elements or compound overlapping with the CdTe and FTO diffractions might be present. Based on the XRD diffraction peak intensity, the (111)C orientation is considered as the preferred orientation of the CdTe layers and the summary of the structural data is captured in Table 1. The extracted XRD data from these CdTe work matches the JCPDS reference file number 01-075-2086-cubic. It should be noted that Scherrer's formula (see equation (1)) was utilised for the calculation of the crystallite size D, where θ is the Bragg angle, β is the full width at half maximum (FWHM) of the diffraction peak in radian and λ is the wavelength of the X-rays used (1.54 Å).

$$D = \frac{0.94\lambda}{\beta \cos\theta} \qquad (1)$$

As observations in Figure 2(g) and Table 1, the highest and the least peak intensity was observed for the glass/FTO/*n*-ZnS/*n*-CdS/*n*-CdTe layers activated with pH2 and pH1 GCT respectively. The comparatively low (111)C diffraction intensity observed for the layers activated with pH3 and pH1 GCT might be due to the richness of Cd and Te in the CdTe layers and compared to the that activated with pH2 GCT. Consequently, the highest

crystallinity of 65.4 nm was observed for the layers activated with pH2 GCT. It should be noted that the crystallite size as calculated using XRD does not correspond to the grain size as seen on the SEM micrograph but the grains are formed from several crystallites.

Table 1: Summary of the X-ray diffraction analysis for cubic (111) CdTe diffraction.

Acidity	2θ (°)	Peak intensity (arb. unit)	d-spacing (Å)	FWHM (°)	Crystallite size (nm)
pH3	23.97	809	3.709	0.162	52.3
pH2	23.91	1451	3.718	0.129	65.4
pH1	24.03	358	3.699	0.162	52.3

4 The effects of pH value of the $CdCl_2$+$Ga_2(SO_4)_3$ treatment solution on properties of solar cells

It should be noted that the melting point of CdTe is 1093°C. Therefore, during $CdCl_2$ treatment, large columnar grown crystals of CdTe remain as solids (Amarasinghe et al., 2018; Donghwan Kim et al., 1994; Harvey et al., 2015; Moutinho et al., 1998). However, the presence of the impurities such as excess Cd, excess Te, Cl, O and Ga accumulate in grain boundaries as a result of multi-element segregation after annealing process (Emziane et al., 2005; Harvey et al., 2015; Mao et al., 2014; Mazzamuto et al., 2008; Tuteja et al., 2016), and the melting point of grain boundary material reduces drastically to ~385±5°C (Dharmadasa et al., 2014). Above this temperature, solid CdTe crystals float in a liquid of grain boundary materials, grains grow by Oswald ripening, dope the surface of CdTe crystals using Cl and Ga, and freeze improving the material in grain boundaries after cooling. This process improves the main rectifying contact parallel to the TCO, and produce transverse p-n junctions across the CdTe cylindrical surfaces. This additional *p*-*n* junctions help to separate photo-generated e-h pairs instantly to travel in two different paths. One carrier travels through the CdTe crystal and the other carrier travel through the grain boundary normal to the TCO layer minimising recombination. This is known as grain boundary enhanced PV effect and the full description can be found in a previous publication (Dharmadasa, 2014; Dharmadasa et al., 2014; Dharmadasa and Ojo, 2017).

Figure 4 (a) depicts the J-V curves recorded for the glass/FTO/*n*-ZnS/*n*-CdS/*n*-CdTe/Au devices fabricated from the pH1, pH2 and pH3 GCT layers measured under AM1.5 condition. Figure 4 (b) and Figure 4 (c) show the graph of capacitance against bias voltage and the corresponding Mott–Schottky plot for the devices fabricated from the pH1 GCT glass/FTO/n-ZnS/n-CdS/n-CdTe/Au devices. Figure 4 (d) and Figure 4 (e) show the graph of

capacitance against bias voltage and the corresponding Mott–Schottky plot for the device fabricated from the pH2 GCT glass/FTO/n-ZnS/n-CdS/n-CdTe/Au devices. The measured device summary is captured in Table 2. The effective Richardson constant (A^*) utilised for calculations has been predetermined as 12 $Am^{-2}K^{-2}$ for CdTe using Eq (2).

$$A^* = \frac{4\pi m^* k^2 q}{h^3} \qquad (2)$$

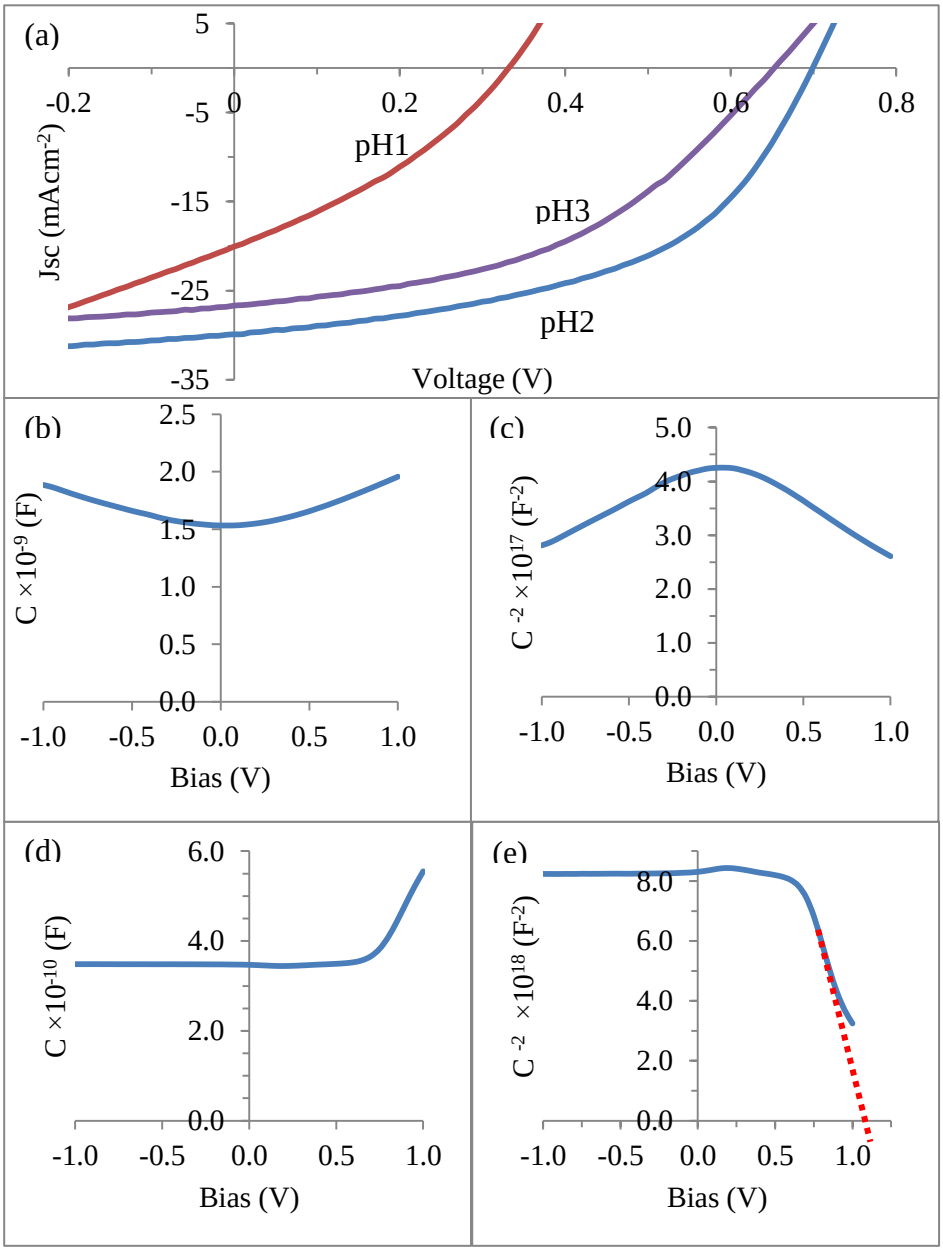

Figure 4: (a) Typical current–voltage curves of the glass/FTO/*n*-ZnS/*n*-CdS/*n*-CdTe/Au devices treated with pH1, pH2 and pH3 GCT, (b) Capacitance-voltage plot and (c) Schottky-Mott plot under dark conditions for the cell fabricated from the pH1 GCT layers, (d) Capacitance-voltage plot and (d) Schottky–Mott plot under dark conditions for the cells fabricated from the pH2 GCT layers.

As depicted in the J-V section of Table 2, shunt resistance (R_{sh}) >1 MΩ were recorded for the glass/FTO/n-ZnS/n-CdS/n-CdTe/Au devices activated with pH2 and pH3 as compared to the low R_{sh} value of the pH1 GCT treated case. It should be noted that low R_{sh} values of fabricated photovoltaic devices can be attributed to low semiconductor material quality to the presence of pinholes, gaps, voids, and high dislocation density within the semiconductor material (Soga, 2006) amongst others. It is not surprising that low R_{sh} value for the devices fabricated from the pH1 glass/FTO/n-ZnS/n-CdS/n-CdTe GCT layers was observed due to the eroded morphology and the optical summation as discussed in Section 3. Further to this, rectification factor (*RF*) values higher than 3 orders of magnitude was observed for the glass/FTO/n-ZnS/n-CdS/n-CdTe/Au activated with pH2 and pH3 GCT. As documented in the literature, *RF* values equal or higher than 2.5 orders of magnitude is a characteristic property of high-efficiency solar cells (Dharmadasa, 2013). The severe reduction in the *RF* value for the devices fabricated from the pH1 GCT treated glass/FTO/*n*-ZnS/*n*-CdS/*n*-CdTe can be ascribed to the CdTe material deterioration due to the harshness of the acidic dissolution of Cd from the CdTe surface and the resulting surface erosion of the CdTe surface as discussed in Section 3.

Likewise, the ideality factor (*n*) of the devices fabricated from the pH2 and pH3 GCT treated glass/FTO/*n*-ZnS/*n*-CdS/*n*-CdTe lies between 1.00 and 2.00, while the *n* values for the pH1 treated layers were >2.00. This signifies that the dominating current transport mechanism of the devices fabricated from the glass/FTO/*n*-ZnS/*n*-CdS/*n*-CdTe activated with pH2 and pH3 GCT is by both thermionic emission and recombination & generation (R&G) processes in parallel. While the *n* value >2.00, observed for the devices fabricated from the pH1 GCT layers signifies that the current transportation mechanism is dominated by R&G and the tunnelling of high energy electron through the barrier height (Verschraegen et al., 2005), which consequentially results in the reduction of the barrier height ϕ_b as depicted in Table 2.

With reference to Figure 4 (a) and the (AM1.5 illuminated condition) J-V section of Table 2, short circuit current density (J_{sc}) higher than the Shockley-Queisser limit for single *p*-*n* junction (Shockley and Queisser, 1961) was observed for the glass/FTO/*n*-ZnS/*n*-CdS/*n*-CdTe/Au devices fabricated from the pH2 and pH3 GCT treated layers. The high J_{sc} can be attributed to the multi-junction graded bandgap *n*-*n*-*n*+*SB* device configuration (Vos, 2000). To ascertain the authenticity of the parameters measured, the cells under test were isolated by carefully removing surrounding layers to avoid possible peripheral current collection as suggested in the literature (Godfrey and Green, 1977). The collection of current from the periphery is not expected due to the high resistivity and low thickness of ~1300 nm utilised in

this work (Basol, 1984). Further to this, comparatively higher open-circuit voltage (V_{oc}), fill-factor (FF) and efficiency (η) were observed for the devices fabricated from the pH2 and pH3 GCT (but championed by pH2 GCT) as compared to the fabricated device using pH1 GCT treated layer.

Table 2: Summary of device and material parameters obtained from I-V (both under illuminated and dark conditions) and C-V (dark condition) for glass/FTO/*n*-ZnS/*n*-CdS/*n*-CdTe/Au solar cells activated with pH1, pH2 and pH3 GCT treatment.

GCT pH	pH1.00	pH2.00	pH3.00
J-V under dark condition			
R_{sh} (Ω)	9230.7	$>10^6$	$>10^6$
R_s (kΩ)	1.25	0.66	0.84
R.F	$10^{0.6}$	10^4	$10^{3.8}$
I_o (A)	3.16×10^{-6}	1.25×10^{-9}	1.99×10^{-9}
n	>2.00	1.67	1.82
Φ_b (eV)	>0.56	>0.81	>0.79
I-V under 1.5 AM illumination condition			
R_{sh} (Ω)	236	162	310
R_s (Ω)	952	4000	4285
I_{sc} (mA)	0.63	0.96	0.85
J_{sc} ($mAcm^{-2}$)	20.06	30.57	27.07
V_{oc} (V)	0.340	0.710	0.650
Fill factor	0.31	0.56	0.51
Efficiency (%)	2.11	12.16	8.97
C-V under dark condition			
σ $(\Omega.cm)^{-1}$	1.14×10^{-3}	3.60×10^{-3}	9.80×10^{-4}
N_D (cm^{-3})	6.22×10^{16}	1.12×10^{15}	7.80×10^{14}
μ ($cm^2V^{-1}s^{-1}$)	0.11	20.06	7.84
C_o (pF)	1500	350	283
W (nm)	203.9	873.8	1080.6

The C-V measurements presented in Figure 4 (b-e) and Table 2 were performed under dark condition at a frequency of 1.0 MHz AC signal, bias range of (-1.00 to 1.00) V at 300 K. The doping density (N_D) and built-in potential (V_{bi}) for this devices were determined using the

Mott-Schottky plot as shown in Figure 4 (c) and Figure 4 (e) for the devices incorporated layers activated with pH1 and pH2 GCT respectively. Equations (3) to (5) were also utilised.

$$\frac{1}{C^2} = \frac{2}{\varepsilon_s e A^2 N_D}\left(V_R + V_{bi}\right) \tag{3}$$

$$Slope = \frac{2}{\varepsilon_s e N_D A^2} \tag{4}$$

$$N_D = \frac{2}{\varepsilon_r \varepsilon_0 e A^2 \times slope} \tag{5}$$

where C is the capacitance, ε_r is the relative dielectric constant, ε_o is the permittivity of free space, ε_s is the semiconductor permittivity, e is the electronic charge, A is the area of the contact, N_D is the donor concentration, V_{bi} is the built-in potential and V_R is the reverse bias voltage. The slope and the intercept of the C^{-2} versus V plot are given by equation (3). The ε_r value utilised for calculation was 11.0 (Strzalkowski et al., 1976), while the calculated effective density of states of the conduction band (N_c) using equation (6) was 9.16×10^{17} cm^{-3}, where, h is the plank's constant, T is the temperature, k is the Boltzmann's constant and m_e^* is the effective electron mass.

$$N_C = 2\left[\frac{2\pi m_e^* kT}{h^2}\right]^{3/2} \tag{6}$$

With the assumption that all donor atoms are ionised at 300 K (therefore $n \approx N_D$), the carrier mobility $\mu_\perp$ was evaluated using equation (7), where σ is the electrical conductivity. Other calculated parameters are shown in Table 2.

$$\mu_\perp = \frac{\sigma}{ne} = \frac{\sigma}{N_D e} \tag{7}$$

As depicted in Table 2, the doping concentration of the devices fabricated from both the pH2 and pH3 GCT treated glass/FTO/*n*-ZnS/*n*-CdS/*n*-CdTe layers lies within the region corresponding to the high-efficiency CdTe devices ~($1.0\times10^{14} - 5\times10^{15}$) cm^{-3} reported in the literature (Britt and Ferekides, 1993; Woodcock et al., 1991). An increase in the doping concentration of the fabricated devices from the pH1 GCT treated glass/FTO/*n*-ZnS/*n*-CdS/*n*-CdTe layers to ~10^{16} cm^{-3} was observed. The high doping concentration recorded for the activated layers using pH1 GCT results in the reduction in the depletion width, loss of short-circuit current density and increment in defect density and the reduction in the photo-generated current (Coutts and Naseem, 1985). As observed from the C-V section of Table 1 and the Mott–Schottky plots as depicts in Figure 4, the devices activated using pH1 GCT

shows a deviation from the linearity as a result of the effects of defects, traps, surface states, interfacial resistive layers (attributable to oxidation) producing excess capacitance and inhomogeneity (Chaure et al., 2003). For the devices fabricated from the pH2 GCT treated glass/FTO/*n*-ZnS/*n*-CdS/*n*-CdTe layers, full depletion at reverse biased and close to zero biased voltages were observed. As shown in Figure 4 (e), an increase in the voltage towards forward bias ~0.6 V, the depletion width W equals the device thickness of ~1300 nm. Above ~0.6 V, an increase in capacitance results was observed with increasing forward bias voltage resulting into a gradual reduction in the depletion width. This observation is in accordance with the Mott–Schottky theory and can be utilised for the estimation of the diffusion voltage of the device (V_{bi}) and the excess donor concentration (N_D-N_A) for *n*-CdTe layer. Increase in the mobility of the devices fabricated from the glass/FTO/*n*-ZnS/*n*-CdS/*n*-CdTe layers activated with pH3 and pH2 but with an increase in acidity to pH1 a reduction in the mobility was observed. The comparatively lower $\mu_{\perp}$ for the devices from the pH1 GCT layers treated might be due to presence of high defects density, R&G centres and tunnelling paths as portrayed by the high ideality factor on the devices and the detrimental effect of the high acidity (low pH≤1) on the material properties (see Section 3).

5 Conclusion

Solar cells (glass/FTO/*n*-ZnS/*n*-CdS/*n*-CdTe/Au) of different GCT activation pH were successfully fabricated and both the material and device properties were explored and systematically presented. Subject to both the material and electronic parameters observed, the optimised pH value of the GCT ($CdCl_2$+$Ga_2(SO_4)_3$) activation treatment is pH2 with activation at pH3 GCT at close proximity. The pH1 GCT treated layers show comparatively low material quality as depicted in morphological, compositional, optical and structural properties. As a result, the devices fabricated from the pH1 GCT treated layers show low device properties. In other words, metalising on Te-rich CdTe surfaces lead to poor solar cell performance. Work is on-going on improving the metal/semiconductor layers utilised and the incorporation other window/buffer layers to further explore the potential of bandgap grading.

Acknowledgements

Authors would like to thank members of the SHU Solar Energy Group for their contributions to this work. The principal author would also like to thank Sheffield Hallam University, Ekiti State University and TETFund Nigeria for their support to carry out this research.

References

Abdul-Manaf, N.A., Weerasinghe, A.R., Echendu, O.K., Dharmadasa, I.M., 2015. Electro-plating and characterisation of cadmium sulphide thin films using ammonium thiosulphate as the sulphur source. J. Mater. Sci. Mater. Electron. 26, 2418–2429. https://doi.org/10.1007/s10854-015-2700-5

Amarasinghe, M., Colegrove, E., Moseley, J., Moutinho, H., Albin, D., Duenow, J., Jensen, S., Kephart, J., Sampath, W., Sivananthan, S., Al-Jassim, M., Metzger, W.K., 2018. Obtaining Large Columnar CdTe Grains and Long Lifetime on Nanocrystalline CdSe, MgZnO, or CdS Layers. Adv. Energy Mater. 8, 1702666. https://doi.org/10.1002/aenm.201702666

Basol, B.M., 1992. Processing high efficiency CdTe solar cells. Int. J. Sol. Energy 12, 25–35. https://doi.org/10.1080/01425919208909748

Basol, B.M., 1984. High-efficiency electroplated heterojunction solar cell. J. Appl. Phys. 55, 601–603. https://doi.org/10.1063/1.333073

Bosio, A., Romeo, N., Mazzamuto, S., Canevari, V., 2006. Polycrystalline CdTe thin films for photovoltaic applications. Prog. Cryst. Growth Charact. Mater. 52, 247–279. https://doi.org/10.1016/j.pcrysgrow.2006.09.001

Britt, J., Ferekides, C., 1993. Thin-film CdS/CdTe solar cell with 15.8% efficiency. Appl. Phys. Lett. 62, 2851–2852. https://doi.org/10.1063/1.109629

Chaure, N.B., Bordas, S., Samantilleke, A.P., Chaure, S.N., Haigh, J., Dharmadasa, I.M., 2003. Investigation of electronic quality of chemical bath deposited cadmium sulphide layers used in thin film photovoltaic solar cells. Thin Solid Films 437, 10–17. https://doi.org/10.1016/S0040-6090(03)00671-0

Coutts, T.J., Naseem, S., 1985. High Efficiency Indium Tin Oxide/Indium Phosphide Solar Cells. Appl. Phys. Lett. 46, 164–166. https://doi.org/10.1063/1.95723

Dharmadasa, I., Roberts, J., Hill, G., 2005. Third generation multi-layer graded band gap solar cells for achieving high conversion efficiencies—II: Experimental results. Sol. Energy Mater. Sol. Cells 88, 413–422. https://doi.org/10.1016/j.solmat.2005.05.008

Dharmadasa, I.M., 2014. Review of the CdCl2 Treatment Used in CdS/CdTe Thin Film Solar Cell Development and New Evidence towards Improved Understanding. Coatings 4, 282–307. https://doi.org/10.3390/coatings4020282

Dharmadasa, I.M., 2013. Advances in thin-film solar cells. Pan Stanford, Singapore.

Dharmadasa, I.M., 2005. Third generation multi-layer tandem solar cells for achieving high conversion efficiencies. Sol. Energy Mater. Sol. Cells 85, 293–300.

https://doi.org/10.1016/j.solmat.2004.08.008

Dharmadasa, I.M., 1998. Recent developments and progress on electrical contacts to CdTe, CdS and ZnSe with special reference to barrier contacts to CdTe. Prog. Cryst. Growth Charact. Mater. 36, 249–290. https://doi.org/10.1016/S0960-8974(98)00010-2

Dharmadasa, I.M., Bingham, P., Echendu, O.K., Salim, H.I., Druffel, T., Dharmadasa, R., Sumanasekera, G., Dharmasena, R., Dergacheva, M.B., Mit, K., Urazov, K., Bowen, L., Walls, M., Abbas, A., 2014. Fabrication of CdS/CdTe-Based Thin Film Solar Cells Using an Electrochemical Technique. Coatings 4, 380–415. https://doi.org/10.3390/coatings4030380

Dharmadasa, I.M., Blomfield, C.J., Scott, C.G., Coratger, R., Ajustron, F., Beauvillain, J., 1998. Metal/n-CdTe interfaces: A study of electrical contacts by deep level transient spectroscopy and ballistic electron emission microscopy. Solid. State. Electron. 42, 595–604. https://doi.org/10.1016/S0038-1101(97)00296-7

Dharmadasa, I.M., Echendu, O.K., Fauzi, F., Abdul-Manaf, N.A., Olusola, O.I., Salim, H.I., Madugu, M.L., Ojo, A.A., 2017. Improvement of composition of CdTe thin films during heat treatment in the presence of CdCl2. J. Mater. Sci. Mater. Electron. 28, 2343–2352. https://doi.org/10.1007/s10854-016-5802-9

Dharmadasa, I.M., Echendu, O.K., Fauzi, F., Abdul-Manaf, N.A., Salim, H.I., Druffel, T., Dharmadasa, R., Lavery, B., 2015. Effects of CdCl2 treatment on deep levels in CdTe and their implications on thin film solar cells: a comprehensive photoluminescence study. J. Mater. Sci. Mater. Electron. 26, 4571–4583. https://doi.org/10.1007/s10854-015-3090-4

Dharmadasa, I.M., Elsherif, O., Tolan, G.J., 2011. Solar Cells Active in Complete Darkness. J. Phys. Conf. Ser. 286, 012041. https://doi.org/10.1088/1742-6596/286/1/012041

Dharmadasa, I.M., Ojo, A.A., 2017. Unravelling complex nature of CdS/CdTe based thin film solar cells. J. Mater. Sci. Mater. Electron. 28, 16598–16617. https://doi.org/10.1007/s10854-017-7615-x

Dharmadasa, I.M., Ojo, A.A., Salim, H.I., Dharmadasa, R., 2015. Next Generation Solar Cells Based on Graded Bandgap Device Structures Utilising Rod-Type Nano-Materials. Energies 8, 5440–5458. https://doi.org/10.3390/en8065440

Dharmadasa, I.M., Samantilleke, A.P., Chaure, N.B., Young, J., 2002. New ways of developing glass/conducting glass/CdS/CdTe/metal thin-film solar cells based on a new model. Semicond. Sci. Technol. 17, 1238–1248. https://doi.org/10.1088/0268-1242/17/12/306

Donghwan Kim, Pozder, S., Zhu, Y., Trefny, J.U., 1994. Polycrystalline thin film CdTe solar cells fabricated by electrodeposition, in: Proceedings of 1994 IEEE 1st World Conference on Photovoltaic Energy Conversion - WCPEC (A Joint Conference of PVSC, PVSEC and PSEC). IEEE, pp. 334–337. https://doi.org/10.1109/WCPEC.1994.519969

Emtage, P.R., 1962. Electrical Conduction and the Photovoltaic Effect in Semiconductors with Position-Dependent Band Gaps. J. Appl. Phys. 33, 1950–1960. https://doi.org/10.1063/1.1728874

Emziane, M., Durose, K., Romeo, N., Bosio, A., Halliday, D.P., 2005. Effect of CdCl2 activation on the impurity distribution in CdTe/CdS solar cell structures. Thin Solid Films 480–481, 377–381. https://doi.org/10.1016/j.tsf.2004.11.053

Ergen, O., Gilbert, S.M., Pham, T., Turner, S.J., Tan, M.T.Z., Worsley, M.A., Zettl, A., 2016. Graded bandgap perovskite solar cells. Nat. Mater. 16, 522–525. https://doi.org/10.1038/nmat4795

Fernández, P., 2003. Defect structure and luminescence properties of CdTe based compounds. J. Optoelectron. Adv. Mater. 5, 369–388.

Godfrey, R.B., Green, M.A., 1977. Enhancement of MIS solar-cell ''efficiency'' by peripheral collection. Appl. Phys. Lett. 31, 705–707. https://doi.org/10.1063/1.89487

Han, J., Fu, G., Krishnakumar, V., Liao, C., Jaegermann, W., Besland, M.P., 2013. Preparation and characterization of ZnS/CdS bi-layer for CdTe solar cell application. J. Phys. Chem. Solids 74, 1879–1883. https://doi.org/10.1016/j.jpcs.2013.08.004

Harvey, S.P., Teeter, G., Moutinho, H., Al-Jassim, M.M., 2015. Direct evidence of enhanced chlorine segregation at grain boundaries in polycrystalline CdTe thin films via three-dimensional TOF-SIMS imaging. Prog. Photovoltaics Res. Appl. 23, 838–846. https://doi.org/10.1002/pip.2498

Hovel, H.J., Woodall, J.M., 1973. Ga[sub 1−x]Al[sub x]As-GaAs P-P-N Heterojunction Solar Cells. J. Electrochem. Soc. 120, 1246. https://doi.org/10.1149/1.2403671

Konagai, M., Takahashi, K., 1975. Graded-band-gap pGa1-xAlxAs-nGaAs heterojunction solar cells. J. Appl. Phys. 46, 3542–3546. https://doi.org/10.1063/1.322083

Li, C., Poplawsky, J., Paudel, N., Pennycook, T.J., Haigh, S.J., Al-Jassim, M.M., Yan, Y., Pennycook, S.J., 2014. S-Te Interdiffusion within Grains and Grain Boundaries in CdTe Solar Cells. IEEE J. Photovoltaics 4, 1636–1643. https://doi.org/10.1109/JPHOTOV.2014.2351622

Liu, H., Tian, Y., Zhang, Y., Gao, K., Lu, K., Wu, R., Qin, D., Wu, H., Peng, Z., Hou, L.,

Huang, W., 2015. Solution processed CdTe/CdSe nanocrystal solar cells with more than 5.5% efficiency by using an inverted device structure. J. Mater. Chem. C 3, 4227–4234. https://doi.org/10.1039/C4TC02816C

Madugu, M.L., Olusola, O.I.-O., Echendu, O.K., Kadem, B., Dharmadasa, I.M., 2016. Intrinsic Doping in Electrodeposited ZnS Thin Films for Application in Large-Area Optoelectronic Devices. J. Electron. Mater. 45, 2710–2717. https://doi.org/10.1007/s11664-015-4310-7

Major, J.D., Al Turkestani, M., Bowen, L., Brossard, M., Li, C., Lagoudakis, P., Pennycook, S.J., Phillips, L.J., Treharne, R.E., Durose, K., 2016. In-depth analysis of chloride treatments for thin-film CdTe solar cells. Nat. Commun. 7, 13231. https://doi.org/10.1038/ncomms13231

Major, J.D., Bowen, L., Treharne, R.E., Phillips, L.J., Durose, K., 2015. NH 4 Cl Alternative to the CdCl 2 Treatment Step for CdTe Thin-Film Solar Cells. IEEE J. 5, 386–389. https://doi.org/10.1109/JPHOTOV.2014.2362296

Mao, D., Wickersham, C.E., Gloeckler, M., 2014. Measurement of Chlorine Concentrations at CdTe Grain Boundaries. IEEE J. Photovoltaics 4, 1655–1658. https://doi.org/10.1109/JPHOTOV.2014.2357258

Mazzamuto, S., Vaillant, L., Bosio, A., Romeo, N., Armani, N., Salviati, G., 2008. A study of the CdTe treatment with a Freon gas such as CHF2Cl. Thin Solid Films 516, 7079–7083. https://doi.org/10.1016/j.tsf.2007.12.124

McCandless, B.E., Sites, J.R., 2011. Cadmium Telluride Solar Cells, in: Handbook of Photovoltaic Science and Engineering. John Wiley & Sons, Ltd, Chichester, UK, pp. 600–641. https://doi.org/10.1002/9780470974704.ch14

Mis-Fernández, R., Rimmaudo, I., Rejón, V., Hernandez-Rodriguez, E., Riech, I., Romeo, A., Peña, J.L., 2017. Deep study of MgCl 2 as activator in CdS/CdTe solar cells. Sol. Energy 155, 620–626. https://doi.org/10.1016/j.solener.2017.06.061

Moutinho, H.R., Al-Jassim, M.M., Levi, D.H., Dippo, P.C., Kazmerski, L.L., 1998. Effects of CdCl2 treatment on the recrystallization and electro-optical properties of CdTe thin films. J. Vac. Sci. Technol. A Vacuum, Surfaces, Film. 16, 1251–1257. https://doi.org/10.1116/1.581269

Ojo, A.A., Olusola, I.O., Dharmadasa, I.M., 2017. Effect of the inclusion of galium in normal cadmium chloride treatment on electrical properties of CdS/CdTe solar cell. Mater. Chem. Phys. 196, 229–236. https://doi.org/10.1016/j.matchemphys.2017.04.053

Oladeji, I.O., Chow, L., 2005. Synthesis and processing of CdS/ZnS multilayer films for solar

cell application. Thin Solid Films 474, 77–83. https://doi.org/10.1016/j.tsf.2004.08.114

Olusola, O.I., Madugu, M.L., Ojo, A.A., Dharmadasa, I.M., 2017. Investigating the effect of GaCl3 incorporation into the usual CdCl2 treatment on CdTe-based solar cell device structures. Curr. Appl. Phys. 17, 279–289. https://doi.org/10.1016/j.cap.2016.11.027

Rios-Flores, A., Arés, O., Camacho, J.M., Rejon, V., Peña, J.L., 2012. Procedure to obtain higher than 14% efficient thin film CdS/CdTe solar cells activated with HCF 2Cl gas. Sol. Energy 86, 780–785. https://doi.org/10.1016/j.solener.2011.12.002

Salim, H.I., Patel, V., Abbas, a., Walls, J.M., Dharmadasa, I.M., 2015. Electrodeposition of CdTe thin films using nitrate precursor for applications in solar cells. J. Mater. Sci. Mater. Electron. 26, 3119–3128. https://doi.org/10.1007/s10854-015-2805-x

Sathaye, S.D., Sinha, A.P.B., 1976. Studies on thin films of cadmium sulphide prepared by a chemical deposition method. Thin Solid Films 37, 15–23. https://doi.org/10.1016/0040-6090(76)90531-9

Shockley, W., Queisser, H.J., 1961. Detailed Balance Limit of Efficiency of p-n Junction Solar Cells. J. Appl. Phys. 32, 510. https://doi.org/10.1063/1.1736034

Sochinskii, N.V. V, Babentsov, V.N.N., Tarbaev, N.I.I., Serrano, M.D., Dieguez, E., 1993. The low temperature annealing of p-cadmium telluride in gallium-bath. Mater. Res. Bull. 28, 1061–1066. https://doi.org/http://dx.doi.org/10.1016/0025-5408(93)90144-3

Soga, T., 2006. Nanostructured Materials for Solar Energy Conversion. Elsvier Sci. 614.

Strzalkowski, I., Joshi, S., Crowell, C.R., 1976. Dielectric constant and its temperature dependence for GaAs, CdTe, and ZnSe. Appl. Phys. Lett. 28, 350–352. https://doi.org/10.1063/1.88755

Tauc, J., 1968. Optical properties and electronic structure of amorphous Ge and Si. Mater. Res. Bull. 3, 37–46. https://doi.org/10.1016/0025-5408(68)90023-8

Tauc, J., 1957. Generation of an emf in Semiconductors with Nonequilibrium Current Carrier Concentrations. Rev. Mod. Phys. 29, 308–324. https://doi.org/10.1103/RevModPhys.29.308

Tuteja, M., Koirala, P., Palekis, V., MacLaren, S., Ferekides, C.S., Collins, R.W., Rockett, A.A., 2016. Direct Observation of CdCl 2 Treatment Induced Grain Boundary Carrier Depletion in CdTe Solar Cells Using Scanning Probe Microwave Reflectivity Based Capacitance Measurements. J. Phys. Chem. C 120, 7020–7024. https://doi.org/10.1021/acs.jpcc.6b00874

Verschraegen, J., Burgelman, M., Penndorf, J., 2005. Temperature dependence of the diode ideality factor in CuInS2-on-Cu-tape solar cells. Thin Solid Films 480–481, 307–311.

https://doi.org/10.1016/j.tsf.2004.11.006

Vos, A. De, 2000. Detailed balance limit of the efficiency of tandem solar cells. J. Phys. D. Appl. Phys. 13, 839–846. https://doi.org/10.1088/0022-3727/13/5/018

Williams, B.L., Major, J.D., Bowen, L., Keuning, W., Creatore, M., Durose, K., 2015. A Comparative Study of the Effects of Nontoxic Chloride Treatments on CdTe Solar Cell Microstructure and Stoichiometry. Adv. Energy Mater. 5, 1–10. https://doi.org/10.1002/aenm.201500554

Williams, B.L., Major, J.D., Bowen, L., Phillips, L., Zoppi, G., Forbes, I., Durose, K., 2014. Challenges and prospects for developing CdS/CdTe substrate solar cells on Mo foils. Sol. Energy Mater. Sol. Cells 124, 31–38. https://doi.org/10.1016/j.solmat.2014.01.017

Wolf, M., 1960. Limitations and Possibilities for Improvement of Photovoltaic Solar Energy Converters: Part I: Considerations for Earth's Surface Operation. Proc. IRE 48, 1246–1263. https://doi.org/10.1109/JRPROC.1960.287647

Woodcock, J.M., Turner, A.K., Ozsan, M.E., Summers, J.G., 1991. Thin film solar cells based on electrodeposited CdTe, in: The Conference Record of the Twenty-Second IEEE Photovoltaic Specialists Conference - 1991. IEEE, pp. 842–847. https://doi.org/10.1109/PVSC.1991.169328

Xue, H., Wu, R., Xie, Y., Tan, Q., Qin, D., Wu, H., Huang, W., 2016. Recent Progress on Solution-Processed CdTe Nanocrystals Solar Cells. Appl. Sci. 6, 197. https://doi.org/10.3390/app6070197